



HAL
open science

Deep mutational scanning of the *Neisseria meningitidis* major pilin reveals the importance of pilus tip-mediated adhesion

Paul Kennouche, Arthur Charles-orszag, Daiki H Nishiguchi, Sylvie Goussard, Anne-flore Imhaus, Mathieu Dupré, Julia Chamot-rooke, Guillaume Duménil

► To cite this version:

Paul Kennouche, Arthur Charles-orszag, Daiki H Nishiguchi, Sylvie Goussard, Anne-flore Imhaus, et al.. Deep mutational scanning of the *Neisseria meningitidis* major pilin reveals the importance of pilus tip-mediated adhesion. *EMBO Journal*, 2019, 10.15252/emj.2019102145 . pasteur-02332462

HAL Id: pasteur-02332462

<https://pasteur.hal.science/pasteur-02332462v1>



Submitted on 31 Oct 2019

HAL is a multi-disciplinary open access archive for the deposit and dissemination of scientific research documents, whether they are published or not. The documents may come from teaching and research institutions in France or abroad, or from public or private research centers.

L'archive ouverte pluridisciplinaire **HAL**, est destinée au dépôt et à la diffusion de documents scientifiques de niveau recherche, publiés ou non, émanant des établissements d'enseignement et de recherche français ou étrangers, des laboratoires publics ou privés.

Copyright

Deep mutational scanning of the *Neisseria meningitidis* major pilin reveals the importance of pilus tip-mediated adhesion

Paul Kennouche^{1,2}, Arthur Charles-Orszag¹, Daiki Nishiguchi¹ , Sylvie Goussard¹, Anne-Flore Imhaus¹, Mathieu Dupré³, Julia Chamot-Rooke³ & Guillaume Duménil^{1,*} 

Abstract

Type IV pili (TFP) are multifunctional micrometer-long filaments expressed at the surface of many prokaryotes. In *Neisseria meningitidis*, TFP are crucial for virulence. Indeed, these homopolymers of the major pilin PilE mediate interbacterial aggregation and adhesion to host cells. However, the mechanisms behind these functions remain unclear. Here, we simultaneously determined regions of PilE involved in pilus display, auto-aggregation, and adhesion by using deep mutational scanning and started mining this extensive functional map. For auto-aggregation, pili must reach a minimum length to allow pilus–pilus interactions through an electropositive cluster of residues centered around Lys140. For adhesion, results point to a key role for the tip of the pilus. Accordingly, purified pili interacting with host cells initially bind via their tip-located major pilin and then along their length. Overall, these results identify functional domains of PilE and support a direct role of the major pilin in TFP-dependent aggregation and adhesion.

Keywords bacterial adhesion; deep mutational scanning; meningitis; pilin; type IV pilus

Subject Categories Cell Adhesion, Polarity & Cytoskeleton; Microbiology, Virology & Host Pathogen Interaction

DOI 10.15252/emj.2019102145 | Received 29 March 2019 | Revised 10 September 2019 | Accepted 12 September 2019

The EMBO Journal (2019) e102145

Introduction

Prokaryotes use a great variety of surface appendages in order to interact with their environment. Type IV filaments (TFP) constitute a class of closely related proteinaceous appendages characterized by a conserved amino-terminal signature sequence of their major constituent, the class III signal peptide (Berry & Pelicic, 2015). They comprise type IV pili (TFP), the bacterial type II secretion

system (T2SS), and the archaellum (archaeal flagellum). Specifically, TFP are micrometer-long retractile and highly dynamic filamentous appendages found at the surface of several pathogenic bacteria such as *Neisseria meningitidis*, *Neisseria gonorrhoeae*, *Pseudomonas aeruginosa*, and *Vibrio cholerae* (Berry & Pelicic, 2015). They mediate several functions including competence for transformation (Seifert *et al.*, 1990), interbacterial aggregation (Blake *et al.*, 1989), twitching motility (Merz *et al.*, 2000), and adhesion to host cells (Woods *et al.*, 1980). The multiple functions mediated by TFP place them as central components in the pathogenicity of these bacteria.

N. meningitidis (or meningococcus), used in this study as a model of TFP-expressing organism, is a diderm bacterium found as a commensal in the human nasopharynx. Occasionally, the bacterium can breach the oropharyngeal epithelial barrier and colonize human blood vessels, eventually leading to sepsis and/or meningitis (van Deuren *et al.*, 2000). In a humanized mouse model, this vascular colonization has been shown to be dependent on the ability of bacteria to adhere to human endothelial cells (Melican *et al.*, 2013), resist shear stress through the reorganization of the host cell plasma membrane (Mikaty *et al.*, 2009), and form fluid aggregates (Bonazzi *et al.*, 2018). All these functions are dependent on the presence of TFP, thus highlighting the importance of this virulence factor in the pathogenesis of *Neisseria meningitidis*.

The mechanism behind the multiple functions carried by TFP remains unclear, including for adhesion and auto-aggregation, which are central to infection. Genetic approaches have pointed to the importance of certain Pil proteins such as PilC1, PilV, and PilX. Because *pilC1* mutants fail to adhere to host cells while retaining normal piliation levels and aggregation properties, this protein was for a time thought to be an adhesin (Rudel *et al.*, 1995; Morand *et al.*, 2004). PilV and PilX are part of a group of proteins designated as minor pilins as they all share a high degree of homology with PilE but are expressed at much lower levels. Mutants in *pilX* or *pilV* genes retain some level of piliation while losing certain functions (Winther-Larsen *et al.*, 2001; Helaine *et al.*, 2005; Mikaty *et al.*, 2009; Imhaus & Dumenil, 2014). It has been proposed that

¹ Pathogenesis of Vascular Infections Unit, INSERM, Institut Pasteur, Paris, France

² Université Paris Descartes, Paris, France

³ Institut Pasteur, CNRS USR 2000, Mass Spectrometry for Biology Unit, Paris, France

*Corresponding author. Tel: +33 144389383; E-mail: guillaume.dumenil@inserm.fr

these minor pilins could be inserted periodically in the PilE scaffold and would act as effectors, specifically mediating these functions (Helaine *et al*, 2007; Coureuil *et al*, 2010). A more recent study proposed an alternative hypothesis in which the reduced piliation levels observed in *pilV* and *pilX* mutants, ~70 and ~30% of wild-type levels, are sufficient to explain their phenotypes (Imhaus & Dumenil, 2014). This hypothesis points back to PilE as the central mediator of TFP-associated functions. This implies that PilE is under an unusual number of functional constraints for a 17 kDa protein. First, to assemble retractile TFP, PilE must be able to interact reversibly with several members of the piliation machinery and itself (Georgiadou *et al*, 2012). Second, to support pili bundling and aggregation, PilE must enable interactions between TFP in a parallel and antiparallel fashion. Third, to mediate adhesion, the major pilin needs a region that can interact with components of the host cell surface.

Using a global approach as a starting point, the present study explores the possibility that the pilin itself could directly carry out adhesive and aggregative functions. Saturating mutagenesis approaches have been successfully used in the past in *N. gonorrhoeae* on PorA and the N-terminus of PilE (Chen & Seifert, 2014; Obergfell & Seifert, 2016). We decided to extend this approach by taking advantage of the deep mutational scanning method (Fowler & Fields, 2014) and applied it to the full-length PilE. This provided functional maps of PilE for piliation, aggregation, and adhesion. Mining this extensive dataset and confirming these observations with *de novo*-generated mutant now provides novel insights in the mechanisms underlying TFP-mediated interbacterial aggregation and adhesion to human cells.

Results

Deep mutational scanning of the *Neisseria meningitidis* major pilin PilE

A library of point mutants in the *pilE* gene (sequence type *pilE_{SB}*, Nassif *et al*, 1993) was produced using error-prone PCR and introduced into a strain unable to undergo antigenic variation (guanine quartet mutant, Tan *et al*, 2015). Next-generation sequencing of the genomic *pilE* locus of transformed bacteria revealed that single-point mutations represented 35% of the mutant library and only single mutants were considered for the remainder of the analysis (Fig EV1A–C). Due to the nature of the genetic code, single nucleotide substitutions can theoretically generate four to seven amino acid substitutions. In this context, the library was close to saturation levels, containing 90% of possible amino acid variants (Fig EV1D). On average, every single amino acid of the PilE protein sequence was mutated into 6 alternative amino acids.

This initial library was then submitted to three different carefully validated selection schemes to independently assess surface piliation, auto-aggregation, and adhesion to host cells (Figs 1A and EV1E–I). For the *piliation selection*, live bacteria were immunolabeled with the 20D9 anti-pilus monoclonal antibody (Pujol *et al*, 1999) and sorted by FACS (Fluorescence-Activated Cell Sorting). For the *aggregation selection*, bacterial suspensions from the initial mutant library were allowed to aggregate for 2 h prior to filtration

through transwells with 5- μ m pores. Finally, for the *adhesion selection*, human umbilical vein endothelial cells (HUVEC) were infected with the initial mutant library for 4 h and washed extensively to only retain adherent bacteria. Using next-generation sequencing, the frequency of each single-point mutation in the three selected libraries was compared to the frequency of the same mutation in the initial library. The \log_2 of this ratio is indicative of whether mutations are beneficial or detrimental to the function of interest and was termed *mutation score* (Fig 1A). Overall, 1,147 different point mutations distributed over the whole PilE sequence were associated with three functional quantitative measurements, generating 3,441 data points.

Mutation scores of the stop and synonymous mutations were used to control the validity of the resulting functional mapping. Stop mutations are expected to induce a complete loss of piliation and function, while synonymous mutations should be indistinguishable from the reference strain. Indeed, the majority of stop mutations were negatively selected as shown by their distribution at the left of the volcano plots for the three functions (Fig 1B, blue dots). Conversely, synonymous mutations were distributed evenly around the 0 value (orange dots). Overall, while a large number of mutations affect piliation and associated functions, it is also worth noting that a significant number of mutations have no significant effect or a beneficial effect on pilus expression and functions. This likely reflects the robustness of the piliation system regarding sequence variations. We also observed that the mutation scores for each function were correlated to the mutation scores for piliation (Fig 1C). This is consistent with the observation that piliation is a good predictor of function (Imhaus & Dumenil, 2014) and further validates the strategy.

Mutations in the hyperconserved N-terminal region of the pilin reveal a class of mutants with numerous but short pili that fail to aggregate

Consequently, we first sought mutations that would affect auto-aggregation but not piliation. To tease out such mutants, we compared frequencies between the aggregation library and the piliation library (Fig 2A). Mutations altering auto-aggregation but not piliation could be found all along the sequence (Fig 2A). Mutations in the N-terminal part of the pilin are expected to have strong effects on the piliation level since this conserved region is buried in the core of the pilus structure (Kolappan *et al*, 2016), but mutants with low aggregation and normal piliation levels are unexpected. We thus first focused on the N-terminal part of the protein and undertook a detailed analysis of the piliation of a subset of mutants in the α 1N region with such properties.

Neisseria meningitidis pilE_{L3H}, *pilE_{I4N}*, and *pilE_{V9M}* mutants were generated *de novo* and further studied (Fig 2A, inset 1). Piliation levels of these mutants were first characterized using scanning electron microscopy and immunofluorescence on single bacteria (Fig 2B and C). While the wild-type *pilE_{SB}* strain displayed a few long pili as expected, *pilE_{L3H}*, *pilE_{I4N}*, and *pilE_{V9M}* only expressed numerous very short pili. The frequency of pilated bacteria also seemed increased compared to the wild-type strain. These observations were then confirmed and quantified using flow cytometry (Fig 2D). Analysis of the piliation level of the *pilE_{SB}* reference strain revealed that, in the conditions used here, only around 7% of the

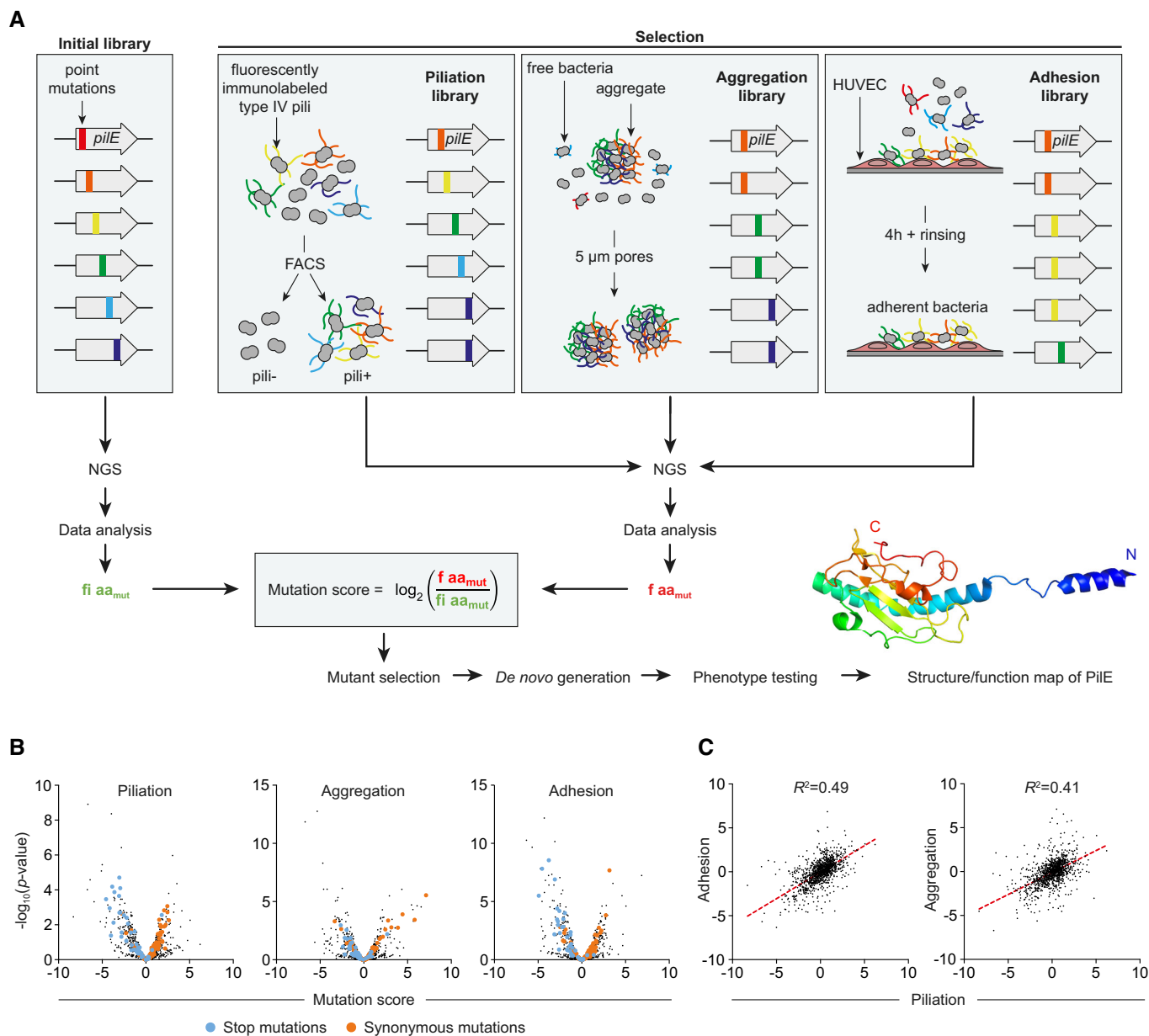


Figure 1. Deep mutational scanning of PilE.

- A Representation of the overall work flow used in the study with the three selection schemes of *pilE* mutants and subsequent NGS-based analysis.
 B Volcano plots of piliation, aggregation, and adhesion mutation scores for all *pilE* mutations. Stop and synonymous mutations are highlighted in blue and orange, respectively.
 C Adhesion and aggregation mutation scores relative to piliation. The correlation appears as a red dotted line.

population is piliated (Fig EV2A–D). Interestingly, conducting this analysis on a large set of *de novo*-generated point mutations as well as the underpiliated *pilX* and the hyperpiliated *pilT* mutants showed a good correlation between the level of piliation per bacterium assessed by flow cytometry and the percentage of piliated bacteria (Fig 2D). In contrast, the *pilE_{L3H}*, *pilE_{I4N}*, and *pilE_{V9M}* mutants were outliers in this distribution with low piliation per bacterium but with a higher percentage of piliated bacteria, reaching an average of 30% in the case of *pilE_{L3H}* (Fig 2D, in green). This phenotype did not result from a change in PilE expression levels as detected by

Western blot (Fig EV2D). Detailed analysis of the piliation of three mutants in the $\alpha 1N$ region of PilE thus reveals that they form a particular class of mutants with a larger proportion of piliated bacteria with short pili.

As expected from the mutational scanning, these *de novo*-generated mutants with short pili showed a near-complete loss of ability to form aggregates (Fig 2E). Mutating the *pilT* retraction ATPase was sufficient to increase piliation of individual bacteria (Fig EV2E) and restore aggregation in mutants with short pili (Fig 2E). This indicates that mutations in these strains do not affect the intrinsic ability of the pili to form

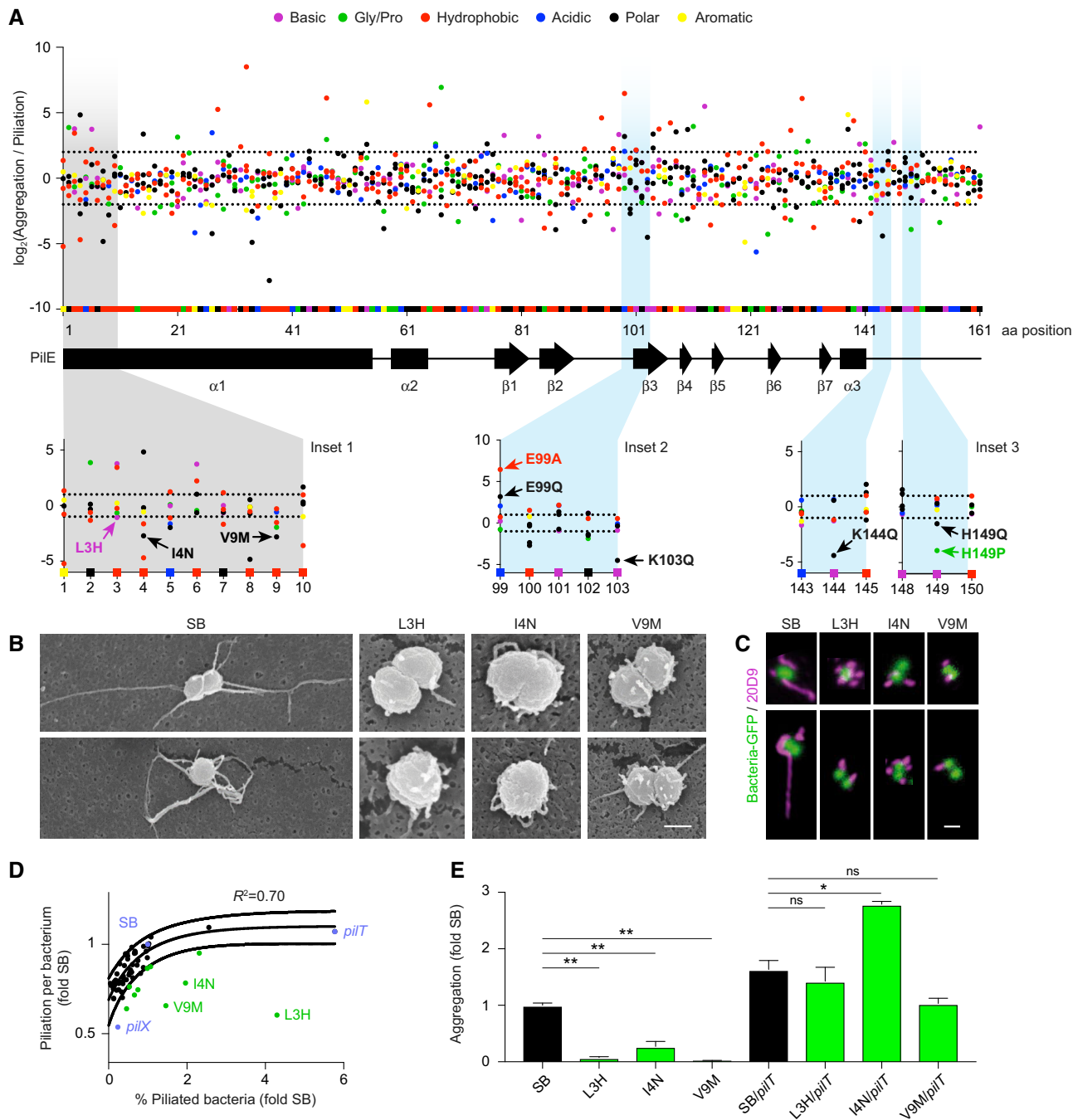


Figure 2. Implication of the amino-terminal region in aggregation.

A The level of aggregation relative to piliation level is represented as the \log_2 of the ratio between the frequency of each single-point mutation in the aggregation library relative to the frequency of the same mutation in the piliation library. Each dot represents a point mutant. Mutation type is color-coded as indicated in the legend. Squares on the x-axis correspond to the original amino acids in the SB sequence with the protein secondary structure indicated below. Dotted lines represent a two-fold threshold value. Bottom insets illustrate the mutations generated *de novo* and further analyzed in Figs 2 and 3.

B Scanning electron microscopy of single bacteria on a cellulose filter. Scale bar: 500 nm.

C Two representative immunofluorescence labeling of TFP. Scale bar: 1 μm .

D Piliation per bacterium as a function of the proportion of piliated bacteria normalized to *pilE_{SB}* values as measured by flow cytometry using the 20D9 monoclonal antibody. Black dots indicate all the individual *de novo*-generated PiIE mutants that were characterized. Blue dots indicate mutants of the piliation machinery and green dots mutants in the $\alpha 1$ N region. Solid lines indicate 95% confidence interval.

E Quantification of aggregation normalized to *pilE_{SB}* for a subset of outliers and corresponding *pilIT* double mutants. Mean values \pm SEM are indicated for each strain. $N \geq 3$ independent experiments. Paired t-test. $P < 0.05$ (*), $P < 0.01$ (**).

pili–pili interactions, and rather suggests that in these strains, pili are too short to form stable interactions. Interestingly, mutants with short but numerous pili not only had no defect in early adhesion, but even had better adhesive properties thus providing further evidence for the functionality of these pili (Fig EV2F). Together, these results support the idea that pilus length is a critical determinant of aggregation and highlight the importance of the N-terminal region of PilE in the balance between pilus length and pilus number.

A patch of charged amino acids surrounding K140 in the C-terminal part of PilE is necessary for aggregation

A second region of interest regarding auto-aggregation is the globular head domain located at the C-terminal end of the pilin. A face of this domain is surface-exposed and has been suggested to be involved in direct pilus–pilus interactions (Kolappan et al, 2016). Since previous studies have indicated the importance of electrostatic interactions between pili (Chamot-Rooke et al, 2011), we focused

on charged amino acids in this area of the protein (Fig 2A, insets 2 and 3). Mutations in three basic residues (K103, K144, and H149) result in a decrease in aggregation, while a mutation in one acidic residue (E99) leads to a strong increase in aggregation. Strikingly, these four amino acids delineate a cavity in the pilus structure, which is overhung by the bulky K140 (Fig 3A). We therefore focused on this patch and generated *de novo* several mutations around K140. Since we suspected that this region might be the epitope recognized by the 20D9 monoclonal antibody used for piliation quantification in the screening strategy, we also used an alternative antibody directed against TFP (F10 nanobody) to assess the piliation levels of these mutants (Charles-Orszag et al, 2018). While there was an excellent agreement between the measurements made with 20D9 and F10 ($R^2 = 0.94$), we found two outliers in this distribution, *pilE*_{Q122E} and *pilE*_{K140Q} (Fig 3B), showing that these two amino acids are important constituents of the 20D9 epitope and that these two mutants present unaffected piliation levels. This observation was confirmed by immunofluorescence (Fig 3C).

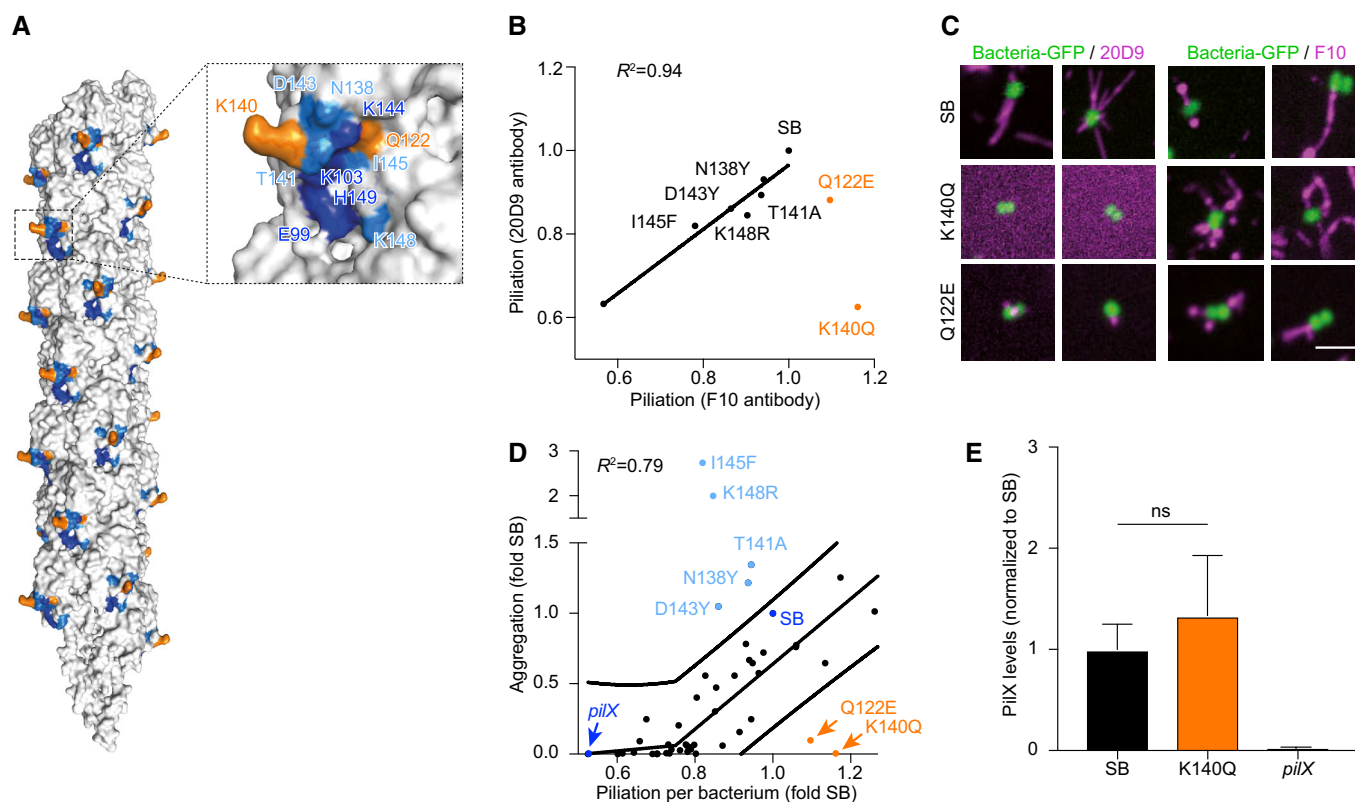


Figure 3. Carboxy-terminal region of the pilin involved in aggregation.

- A Pilus structure (PDB: 5KUA) showing a cluster of charged amino acids surrounding the protruding K140 involved in aggregation. N138 is in light blue; Q122 and K140 in orange; and E99, K103, K144, and H149 in dark blue.
- B Piliation per bacterium as measured by flow cytometry using the 20D9 monoclonal antibody and the F10 nanobody.
- C Visualization of type IV pili by immunofluorescence either using the 20D9 antibody or the F10 nanobody as indicated (magenta). In the case of the K140Q mutant labeled with the 20D9 antibody, the background was made visible to convincingly show the absence of pilus labeling. Scale bar: 2 μ m.
- D Aggregation expressed as a function of piliation per bacterium measured with 20D9 antibody except for *pilE*_{Q122E} and *pilE*_{K140Q} for which the F10 nanobody value is reported. Each dot represents values for a PilE point mutant relative to the SB strain. Hypo-aggregative mutants are highlighted in orange, while hyper-aggregative mutants are in light blue. Solid lines indicate the 95% confidence interval.
- E Quantification of PilX present in purified pili preparations sheared from the bacterial surface using Western blot. PilX levels were normalized using PilE as a reference and normalized to *pilE*_{SB} values. Mean ratio \pm SEM is indicated. $N = 3$ independent experiments. Paired t-test.

We next characterized the auto-aggregation abilities of the mutants in the K140 region. Below a certain piliation threshold, aggregation was lost (Fig 3D) as previously observed in the case of the *pilX* mutant (Imhaus & Dumenil, 2014). Above this threshold, aggregation increases progressively and is correlated with the piliation level. In contrast, mutations located in the K140 region formed two outlying groups: one group with lower aggregative properties (Fig 3D, indicated in orange) and a second with higher aggregation levels (Fig 3D, indicated in blue). This supports the notion that local charge and organization in this region are crucial for aggregation and further indicates a central role of the positive charge of K140 in aggregation. In addition, certain mutants with higher aggregation suggest that the presence of hydrophobic residues on the pilus surface could favor aggregation. Since PilX was described as a direct pilus-associated pro-aggregative factor in some studies (Helaine *et al*, 2005, 2007), the possibility that mutations in the K140 region might affect the association of PilX with pili was tested. Pili were purified by standard methods based on shearing in basic conditions followed by ammonium sulfate precipitation (Chamot-Rooke *et al*, 2007) and the levels of associated proteins evaluated by Western blot. Mutations in the K140 area did not affect PilX copurification (Fig 3E). In addition, this mutation did not alter pilin posttranslational modifications (Table 1). Therefore, the electropositive region centered around K140 in the major pilin is essential for TFP-mediated aggregation.

Mutations specifically affecting adhesion but not aggregation are found at the tip of the pilus

We then analyzed the results of the adhesion library. Various studies have found that the ability of *Neisseria meningitidis* to adhere to human cells is tightly linked to their ability to form aggregates, presumably by allowing the accumulation of bacteria in three dimensions at the site of adhesion (Helaine *et al*, 2005). A central objective of this section was to explore whether regions of PilE specifically involved in adhesion could be identified. The ratio of the mutation score for adhesion over the mutation score for aggregation was thus determined for each mutation (Fig 4A). Averaging the adhesion/aggregation ratio over a window of five consecutive amino acids (magenta line) highlighted two regions with a severe defect in adhesion centered around amino acids Y50 and A131. Interestingly, these amino acids are located in regions of the pilin

monomer found at the tip of the pilus (heat map). In particular, the conserved region surrounding Y50 is part of a EYYLN motif recognized by the SM1 monoclonal antibody and has been shown to only be exposed at the tip of the pilus when these are not under tension (Biais *et al*, 2010; Brissac *et al*, 2012).

To confirm these observations, mutants in these two regions were generated *de novo* and their ability to adhere to human endothelial cells was assessed at 30 min after initial contact. At this early time point, the contribution of aggregation is negligible and the adhesion of individual bacteria remains dependent on the presence of TFP at the bacterial surface as well as on accessory proteins such as PilC1, PilV, and PilX (Fig EV3A–F). Plotting early adhesion levels as a function of aggregation levels highlights mutations with a specific defect in adhesion (Fig 4B). Most interestingly, mutation H54Y showed a strong defect in adhesion while maintaining a near-normal aggregation. Single amino acid mutations in PilE are sufficient to induce a loss of adhesion, thereby exhibiting more specific phenotypes than the *pilV* and *pilC1* deletion mutants. Importantly, these phenotypes were not due to alterations in pili number and length (Figs 4D and E, and EV4A). In addition, the amount of PilV associated with purified pilus fractions was not affected by these mutations (Fig EV4B and C).

Under the hypothesis of a pilus tip-mediated adhesion, a prediction would be that pilus number (i.e., number of pilus tips) is more important than pilus length to promote efficient early adhesion. The piliation level per bacterium as determined by flow cytometry, which is mostly related to pilus length, would thus not correlate with early adhesion. Accordingly, we could not find any significant correlation between the piliation level per bacterium and early adhesion in the mutants characterized in this study (Fig 4C). These results are in contrast to what is observed at 4 h postinfection where aggregation, and thus pilus length, comes into play (Fig EV4D and E).

Overall, this mutational analysis points to the possibility of a tip-mediated adhesion mechanism. At the structural level, amino acids that affect initial adhesion upon mutation form a patch at the pilus tip (Fig 4F).

TFP adhere first by their tip and then along their side

The previous findings prompted us to examine microscopically whether tip-mediated adhesion could be visualized directly. Shear

Table 1. Characterization of non-aggregative pili by mass spectrometry.

Pilin	PTM	M theo.	M exp.	Delta M (ppm)	Relative abundance
PilE _{SB}	Me × 1; GATDH × 1; PG × 1; Disulfide bond × 1	17,479.82	17,479.98	−9.3	100
	Me × 1; GATDH × 1; PG × 2; Disulfide bond × 1	17,633.83	17,633.95	−7.0	86
PilE _{K140Q}	Me × 1; GATDH × 1; PG × 1; Disulfide bond × 1	17,479.79	17,479.95	−9.2	100
	Me × 1; GATDH × 1; PG × 2; Disulfide bond × 1	17,633.79	17,633.92	−7.6	38
PilE _{Q122E}	Me × 1; × 1; PG × 1; Disulfide bond × 1	17,480.81	17,480.93	−7.1	100
	Me × 1; GATGATDH DH × 1; PG × 2; Disulfide bond × 1	17,634.81	17,634.94	−7.3	76

PilE proteins from the reference strain and two non-aggregative mutants (*pilE_{K140Q}* and *pilE_{Q122E}*) were analyzed by liquid chromatography coupled to high-resolution mass spectrometry. Each table summarizes the results obtained for each sample in terms of molecular weight including posttranslational modification composition. M theo is the theoretical mass; M exp, the mass measured experimentally; Me, methyl; PG, phosphoglycerol; GATDH, glyceramido-acetamido trideoxyhexose; DeltaM, the difference between theoretical mass and experimental mass expressed in parts per million relative to theoretical mass; Relative abundance (relative intensity). The most abundant ion in the deconvolved spectrum has a relative abundance of 100%, and the relative abundances of all other peaks of the same spectrum are calculated relative to that one (definition from Proteome Deconvolution 3.0, Thermo Scientific).

generated crude pili preparations were incubated with cells, washed, labeled with a fluorescent nanobody, and imaged by spinning-disk confocal microscopy. With this approach, numerous pili bound to the surface of endothelial cells could be visualized.

Observation of different focal planes (z1-3) provided a three-dimensional view showing rigid 1- to 2- μ m-long pili seemingly attached from one end of the pilus and standing away from the cellular surface (Fig 5A and B). Accordingly, mechanical constraints

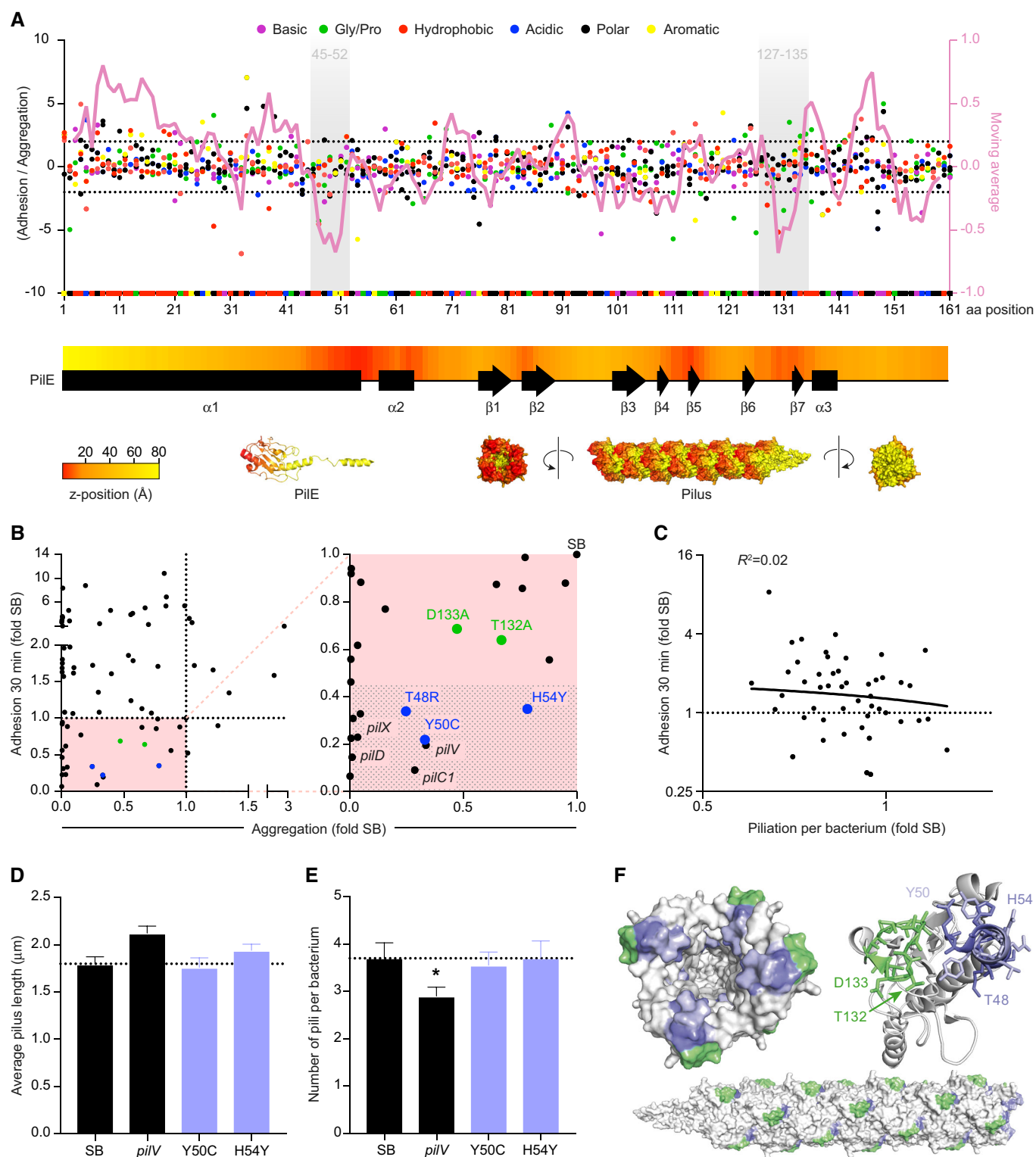


Figure 4.

Figure 4. Residues of the pilin localized toward the distal end of pili are involved in early adhesion.

- A The ratio between the adhesion and aggregation mutation scores for each amino acid in the PilE sequence is represented as dots. Mutation type is color-coded as indicated in the legend. The superimposed magenta line represents the average ratio averaged over a moving window of 5 amino acids (right axis). Shaded areas highlight the two regions identified as important for adhesion. The yellow to red heat map along the pilin sequence indicates the axial position of the amino acid in PilE as shown on the structure of PilE (distal tip in red, proximal tip in yellow).
- B Early adhesion of *pilE* mutants as a function of aggregation. Values were normalized to that of *pilE_{5B}*. Each dot represents a *pilE* mutant and the *pilV*, *pilD*, *pilX*, and *pilC1* reference mutants. Mutants in the region surrounding A131 are in green and those surrounding Y50 in purple. A blown-up view of the zone of interest (lower left quarter) is presented on the right panel. The shaded area highlights the absence of significant adhesion.
- C Early adhesion of PilE mutants as a function of piliation per bacterium normalized to that of *pilE_{5B}*.
- D Piliation length of a selection of mutants determined by immunofluorescence. Average pilus length \pm SEM is indicated. $N = 6$ experiments with at least 50 bacteria analyzed in each experiment. Paired *t*-test.
- E Number of pili per bacteria \pm SEM determined as in (E). Paired *t*-test. $P < 0.05$ (*).
- F Amino acids from the two regions identified in panel (A) are highlighted in purple and green. The SM1 epitope is colored in light purple.

generated by liquid flow led to the bending of pili toward cell surface in the direction of the flow (Fig 5A and B; Movie EV1). Subsequently, the ability of pili to bind along their length was evaluated with increasing flow rates. With shear stress levels below $\sim 5 \text{ dyn cm}^{-2}$, the bending of pili over the cellular surface was reversible and pili moved back to a vertical position when flow was interrupted (Fig 5B and C). In contrast, when flow was applied at a shear stress above $\sim 5 \text{ dyn cm}^{-2}$, pili remained adherent along the cellular surface after the flow was interrupted (Fig 5B and C). This result is in favor of a scenario where pili initially bind to cells by an extremity, tend to remain in a vertical position and when constrained can bind along their side.

The occurrence of adhesion along the length of pili following application of liquid flow could be in favor of force-dependent conformational changes that would expose additional epitopes on the pilus length (Biais *et al*, 2010; Lu *et al*, 2015). Yet, forces exerted on pili in our experimental setup were evaluated (Fig 5D and Appendix) to range between 1 and 4 pN. Such forces would probably not be sufficient to induce the previously described conformational changes that have been estimated to require forces in the tens to hundreds of pN (Beaussart *et al*, 2014; Lu *et al*, 2015). Microscopic observations of the behavior of adherent pili in flow rather suggest that their vertical position is imposed by a restoring torque. To explore whether this explanation is realistic, a physical model was elaborated based on the following assumptions: (i) A 2- μm -long pilus can be modeled as a rigid slender rod since their length is largely below their 5 μm persistence length (Skerker & Berg, 2001); (ii) the rigid rod is considered attached to a plane with a restoring torque bringing it back to its vertical position, and (iii) the pilus rod is under thermal fluctuations (Fig 5D). In this model, increasing shear stress results in the pilus leaning away from its vertical position toward the cell surface (Fig 5E and Appendix). Thermal fluctuations drive the pilus to explore around the equilibrium angle where shear stress and the restoring torque compensate each other, which leads to stochastic adhesion of the pilus along its length. This was sufficient to explain the experimental observations and a single parameter fit reproduced the behavior of pili under flow including the sharp change between reversion to vertical position and adhesion along the pilus length (Fig 5C, red curve), supporting the idea that the adhesion along pilus length is a secondary phenomenon following the initial tip adhesion.

In principle, the purified pili used in this experiment could be interacting with cells through their distal tip or through their hydrophobic proximal base. To distinguish between these two

situations, we used the SM1 monoclonal antibody, which specifically labels the distal tip of the pilus. Indeed, pili adhering on a glass surface only showed labeling by the SM1 antibody at one extremity of the fiber: the distal tip (Fig 5F, arrows). In contrast, on the same fields of view, pili adhered to cells did not display any labeling by the SM1 antibody, suggesting that TFP binding to human endothelial cells masks their distal tip.

Finally, we reasoned that addition of the SM1 antibody to bacteria prior to adhesion, should block the tip of the pilus, and prevent adhesion to host cells. Bacteria were incubated with the SM1 antibody for 15 min prior to adhesion. A dose-dependent inhibition of early adhesion could be observed reaching statistical significance at $20 \mu\text{g ml}^{-1}$ antibody (Fig 5G). Incubation of bacteria with the same amount of the 20D9 monoclonal antibody, which binds along the side of the pili, had no effect on early adhesion, confirming that the effect of the SM1 antibody is not due to lateral binding along the pilus. These data demonstrate that adhesion to human cells is initiated at the tip of the pilus. Importantly, because the SM1 antibody was raised against a sequence present only in the pilin protein, these results strongly support the idea that PilE itself promotes initial adhesion at the tip.

Discussion

Studying TFP functions presents specific challenges, in particular due to their multiple interrelated functions and their highly dynamic nature. In this study, we simultaneously explored three TFP functions in an original and integrated fashion.

A first outcome of this study is the identification of regions of the major pilin involved in bacterial auto-aggregation (Fig 6A–C), a key property that promotes an efficient vascular colonization (Bonazzi *et al*, 2018). Because of the tight link between piliation levels and aggregation, the introduction of a cytometry-based technique to quantify piliation was critical to this investigation. This approach first led to an unexpected observation related to the amino-terminal $\alpha 1\text{N}$ region of PilE. Mutations in this region lead to a particular class of mutants with numerous but short pili that are deficient for aggregation (Fig 6B). These observations suggest that: (i) a minimum pilus length is necessary to enable aggregation and (ii) the $\alpha 1\text{N}$ region is involved in the balance between pilus length and number. The high conservation of this region throughout diverse type IV filaments will provide means to test this hypothesis in various systems. Accordingly, similar mutations in the $\alpha 1\text{N}$ region of

the major pilin of *P. aeruginosa* and *N. gonorrhoeae* have also been shown to lead to defects in microcolony formation (Chiang *et al*, 1995; Park *et al*, 2001). Several mechanisms could account for this new role of the amino-terminus of PilE. This region has been proposed to be involved in regulation of self-expression of the major pilin PilA in *P. aeruginosa* (Kilmury & Burrows, 2016), but it is not the mechanism at play here. We would favor a hypothesis where mutations in the N-terminal part of the protein affect interaction with the piliation machinery. Indeed, in *N. meningitidis*, PilE has been shown to interact with several components of the machinery (PilG, PilN, and PilO) at least partially through its N-terminal

domain (Georgiadou *et al*, 2012). These interactions of the major pilin with the machinery are probably critical for the initiation of pilus assembly, which would then determine the dynamics of extension and retraction.

A second region of PilE required for aggregation is located on the pilus surface around K140. The importance of K140 for pilus bundling and bacterial adhesion had been suggested based on sequence comparison of hyper- and hypo-adherent variants (Marceau *et al*, 1995) and more recently by structural data (Kolappan *et al*, 2016) where it appears as a hook-like structure protruding from the pilus, perhaps allowing the interaction with another pilus. In addition, the

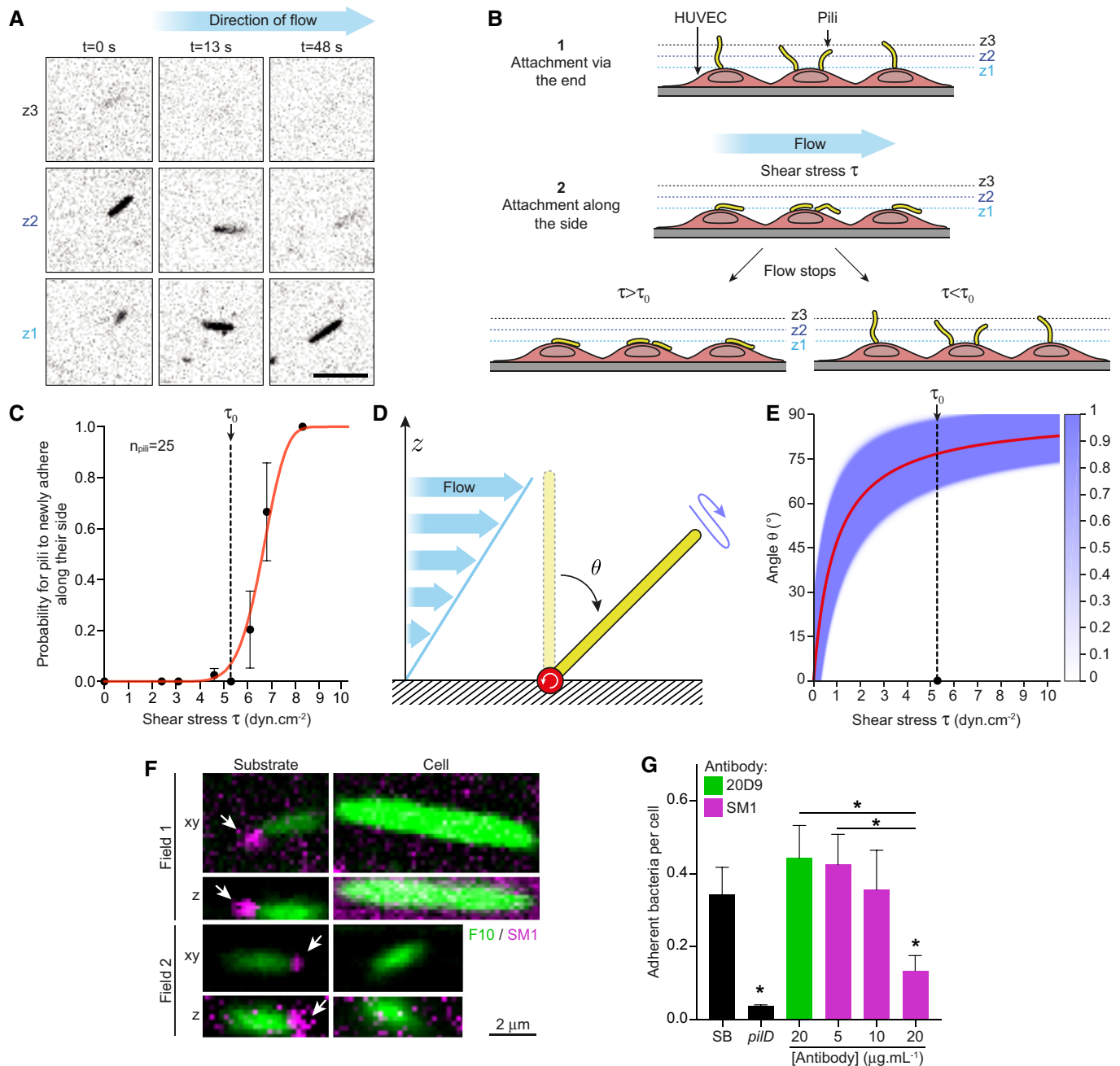


Figure 5.

Figure 5. Interaction of purified type IV pili with cells.

- A Time-lapse of a cell-adhered pilus fluorescently labeled with the F10 nanobody at three different focal planes. Initiation of flow corresponds to $t = 0$. Scale bar: 1 μm . The video presented in Movie EV1.
- B Schematic representation of the experimental setup. Changes in pili position were visualized by imaging different confocal planes (z1-3) using spinning-disk confocal microscopy.
- C Quantification of side adhesion of pili to HUVEC as a function of the shear stress applied. Cell-adhered pili were subjected to gradually increasing flow rates. Each increase was followed by flow arrest and the number of pili adherent along their sides determined. The probability for pili to newly adhere along their side at the i^{th} flow was then calculated as $P_i = 1 - \frac{N_i}{N_{i-1}}$, where N_i is the number of nonadherent pili after the application of the i^{th} flow. $N = 3$ independent experiments. The red curve corresponds to the fit based on the physical model described in the Appendix. Error bars correspond to mean \pm SEM.
- D Schematic representation of the principles of the physical model of a pilus adhering via its tip submitted to shear stress. θ is the angle relative to the vertical position that fluctuates around the equilibrium angle θ_0 due to thermal fluctuations (blue arrow).
- E Probability for the pilus to reach the angle θ during the 30-s application of shear stress τ as determined by the physical model fitted to the data in panel (C). The red line is the equilibrium angle θ_0 and the purple shading the thermal fluctuations.
- F Spinning-disk confocal immunofluorescence of pili stained with both SM1 (magenta) and F10 (green). The thick appearance of TFP is due to the primary and secondary reagents used to detect them as well as diffraction of light. In each field of view, a substrate- and a cell-bound pilus are shown. Upper panels: z-projection from the stacks in the xy plane; bottom panels: side view in the z plane. Scale bar: 2 μm . White arrows correspond to SM1 staining at the tip of pili.
- G Quantification of adhesion after infection of HUVEC cells for 30 min, expressed as the number of adherent bacteria over the number of cell nuclei. Prior to infection, bacteria were incubated at 37°C with or without antibody or nanobody for 15 min. Mean values \pm SEM are indicated for each strain. $N = 5$ independent experiments. Paired *t*-test. $P < 0.05$ (*).

limited sequence conservation of these residues among *N. meningitidis* strains (Fig 6A) could suggest that different structural determinants in this region could participate in aggregation in different strains. The determinants of physiological or pathological protein aggregation have been studied intensively for instance in the context of amyloid fiber formation (De Baets *et al*, 2014). These studies reveal the presence of aggregation-prone regions composed of 5–15 amino acids that tend to auto-aggregate. Similar properties could explain how the major pilin can exhibit a high level of sequence diversity while retaining aggregative properties. More structural and biochemical work on these complex multimeric structures is required to further decipher the molecular mechanism of pilus–pilus interactions.

This study provides several arguments in favor of an adhesion process initiated at the tip of TFP (Fig 6D). First, global mapping of adhesion obtained through deep mutational scanning points to the tip as a key element in early adhesion. Second, early adhesion of pilin mutants in regions exposed at the pilus tip generated *de novo* shows decreased adhesion to human cells. Third, initial adhesion of bacterial cells is inhibited by the SM1 monoclonal antibody, which preferentially binds the tip of the pilus. This monoclonal antibody also binds along the pilus length when pili are under tension, but this is unlikely to have an impact as another monoclonal antibody (20D9), which binds along the pilus length does not inhibit adhesion. Finally, direct microscopic visualization of the adhesion of purified pili to human cells shows that they bind cells via their distal tip. Interestingly, a tip-mediated mechanism of binding has previously been reported in *P. aeruginosa* by imaging fluorescently labeled pili of live bacteria adhering to quartz (Skerker & Berg, 2001; Tala *et al*, 2019).

This also suggests that the pilin itself would be located at the pilus tip and would interact with host cells. The ability of the SM1 antibody directed against a major pilin epitope to inhibit initial bacterial adhesion is in favor of this scenario. The exact nature of the pilus tip is currently unclear, but this result is in contradiction with studies indicating that other proteins such as minor pilins associate with pili and could potentially form the pilus tip. The existence of a structurally distinct pilus tip is well characterized for other pilus type such as the chaperone-usher pilus present in uropathogenic

E. coli (Hospenthal & Waksman, 2019). Electron microscopy images of type I pili show a thin tip fibrillum attached to the pilus itself. This tip contains the adhesin. In type IV pili, however, no identifiable structure has ever been visualized at the tip, thus providing little information. In the case of the *Neisseria spp.*, the PilC1 protein was initially placed at the pilus tip although later studies were in favor of a location in the outer membrane (Rudel *et al*, 1995; Morand *et al*, 2004). Nevertheless, in *Pseudomonas aeruginosa*, PilY1, the PilC1 ortholog copurifies with sheared pili (Nguyen *et al*, 2015). Structural studies in the closely related type II secretion system also suggested that a minor pilin complex composed of GspIJK could fit at the pseudopilus tip (Korotkov & Hol, 2008). Transposed in the piliation system, this study suggested that the orthologous proteins PilI, J, and K could be located at the pilus tip. This idea is strengthened by evidence for pilus association of these minor pilins in *P. aeruginosa* (Giltner *et al*, 2010). A third group of proteins could also be present at the pilus tip, the non-core minor pilin PilV, PilX, and ComP. These proteins co-purify with pili and play a role in adhesion, aggregation, and competence (Nassif *et al*, 1994; Wolfgang *et al*, 1999; Winther-Larsen *et al*, 2001; Helaine *et al*, 2005; Mikaty *et al*, 2009). Overall, evidence of tip location of these proteins is indirect, but if such proteins fully covered the tip of TFP, we should not observe inhibition of adhesion by the SM1 antibody as it specifically binds PilE. Given the multimeric nature of the pilus structure, one cannot exclude, however, the presence of proteins in combination with PilE at the pilus tip. Nevertheless, the inhibitory effect of the SM1 antibody we observe opens new therapeutic opportunities. In the case of non-typeable *Haemophilus influenzae* infection, antibodies directed against the major type IV pilin triggered biofilm dispersion and immunization against the protein offered protection in a mouse model of otitis media (Novotny *et al*, 2015).

Observation of purified pili incubated with host cells under flow also revealed a second type of adhesion that occurs along the length of the pilus (Fig 6D). Purified pili initially interact through their tips and in the absence of flow strikingly stand away from the cell surface. This behavior likely reflects the flexibility of the particular interface formed by the pilus tip and its receptors at the cell surface as well as the relative rigidity of the pilus. Consistently, the 5 μm

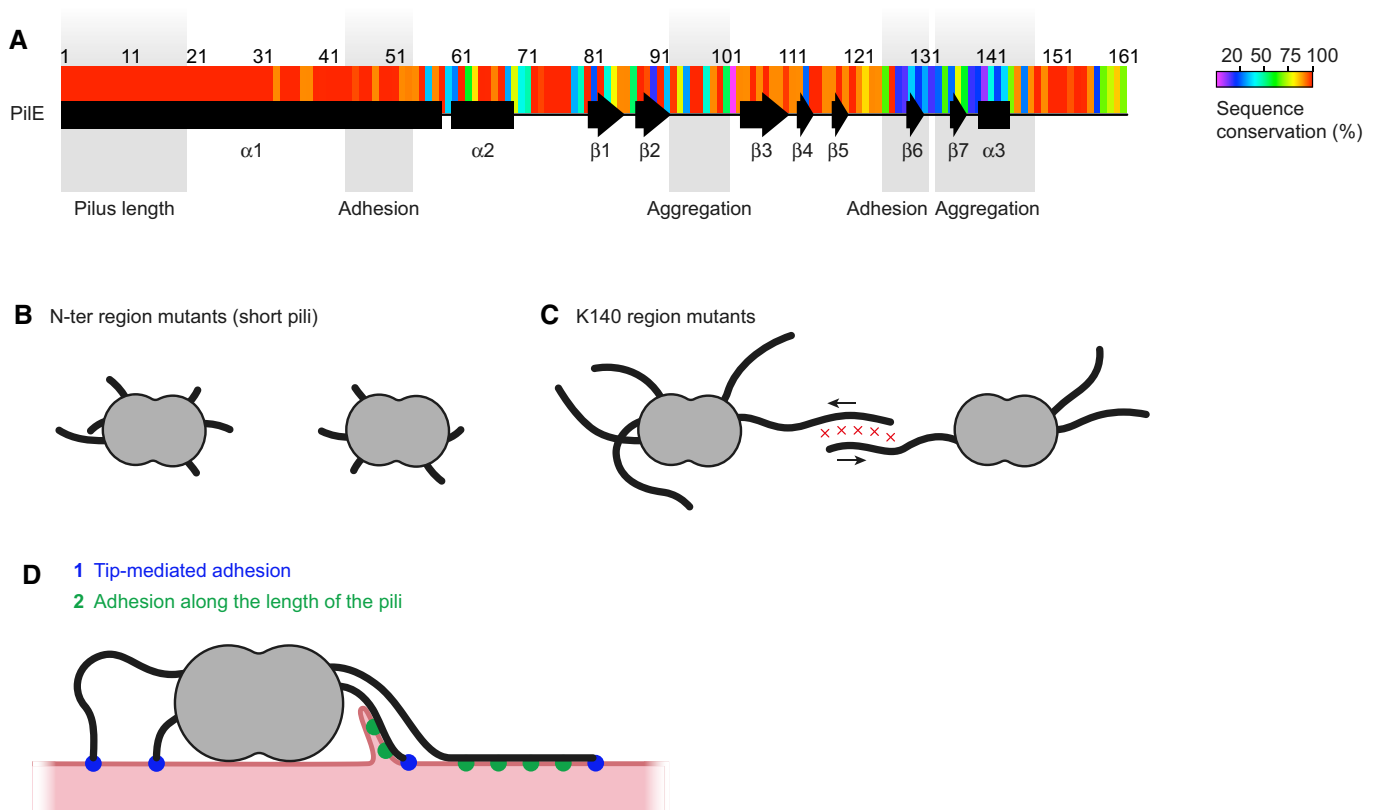


Figure 6. Regions of the major pilin involved in the multiple functions of TFP.

- A Sequence conservation determined from the BIGSdb database of *Neisseria meningitidis* sequences is represented as a heat map (Jolley & Maiden, 2010). Regions of the protein involved in different functions as defined by this study are indicated as shaded areas.
- B A category of mutants in the $\alpha 1$ N amino-terminal region of the pilin express numerous but short pili and fail to auto-aggregate.
- C Pilus-pilus interactions initiating bacterial auto-aggregation fail to occur in mutations affecting the area around K140. Arrows indicate pilus retraction.
- D When in contact with cells, pili can interact through their tips (1) and then along their sides (2). Adhesion of the plasma membrane along the side of the pili mediates one-dimensional wetting and membrane protrusion formation (Charles-Orszag et al, 2018).

persistence length measured for *P. aeruginosa* TFP is longer than the sheared pili used here that are typically 2 μm in length (Skerker & Berg, 2001; Tala et al, 2019). It takes a liquid flow with a shear stress of a few dyn cm^{-2} to bend the pilus to adhere to the cellular surface, thus allowing a second form of adhesion. The molecular basis for this second adhesion remains unclear. One hypothesis could be that flow-induced shear stress could stretch pili and uncover new cell binding sites along the length of the pilus fiber, but calculations suggest that this is unlikely to occur (Beaussart et al, 2014; Lu et al, 2015). Binding along the pilus fiber on the cellular surface evidenced here supports the recently described one-dimensional wetting process that promotes plasma membrane remodeling (Fig 6D) and depends on adhesion along the pilus nanofiber (Charles-Orszag et al, 2018). The specific pilin amino acids involved in this second interaction remain to be identified.

The approach used here provides a framework to explore the numerous multifunctional type four filaments found in bacteria and archaea. In the particular context of *Neisseria meningitidis* infection, this approach led to the identification of the specific structural domains of the major pilin involved in a sequence of events leading to infection: tip-mediated adhesion, adhesion along the length of the

pili followed by bacterial proliferation associated with auto-aggregation mediated by pilus-pilus interactions.

Materials and Methods

Antibodies and chemicals

The following antibodies were used for Western blots and immunofluorescence: (i) polyclonal serum anti-PilE (Morand et al, 2004), anti-PilV (Mikaty et al, 2009), and anti-Rmp4 (Morand et al, 2001); (ii) mouse monoclonal antibody anti-PilE, clone 20D9 (Pujol et al, 1999) and clone SM1 (Virji et al, 1983); (iii) Camelidae nanobody anti-PilE clone F10 (Charles-Orszag et al, 2018). The following goat secondary antibodies were used for immunofluorescence, Western blot, and flow cytometry: anti-mouse or anti-rabbit IgG (H+L) coupled to horseradish peroxidase (Jackson Immuno-Research Laboratories) and anti-rabbit or anti-mouse IgG (H+L) coupled to Alexa Fluor 488, 568, or 647 (Life Technologies) and mouse anti-His tag (Biolegend). 4',6-diamidino-2-phenylindole (DAPI) was purchased from Life Technologies and Hoechst 33342

from Invitrogen. Trypsin-EDTA (0.05%) was purchased from Gibco.

Bacterial growth conditions and mutagenesis

Neisseria meningitidis

8013/clone 12 (2C43) strain expressing the SB pilin variant was used in this study (Nassif *et al*, 1993). In particular, a strain containing a deletion of the guanine quartet upstream of the *pilE* gene (Tan *et al*, 2015) was used to minimize antigenic variation (see below for the construction of this strain). Bacteria were grown on Gonococcus Medium Base (GCB, Difco) agar plates supplemented with Kellogg's supplements (Kellogg *et al*, 1968) and, when required, 100 $\mu\text{g ml}^{-1}$ kanamycin, 2 $\mu\text{g ml}^{-1}$ erythromycin, 50 $\mu\text{g ml}^{-1}$ spectinomycin, or 5 $\mu\text{g ml}^{-1}$ chloramphenicol, at 37°C in moist atmosphere containing 5% CO₂. Before adhesion and aggregation assays, bacteria were grown with shaking at 37°C and 5% CO₂. Bacteria were inoculated at an OD_{600 nm} of 0.05 in Human Endothelial-SFM (Gibco) supplemented with 10% heat-inactivated FBS and grown for 2 h-2 h 30. *Escherichia coli* XL-1 Blue was grown at 37°C on liquid or solid Luria-Bertani medium (Difco) containing 20 $\mu\text{g ml}^{-1}$ chloramphenicol, 50 $\mu\text{g ml}^{-1}$ spectinomycin, 30 $\mu\text{g ml}^{-1}$ kanamycin, or 200 $\mu\text{g ml}^{-1}$ erythromycin when necessary. The guanine quartet mutant was generated as described by Tan and colleagues (Tan *et al*, 2015) using fusion PCR with primers PK-30, 31, 32, and 33 and a chloramphenicol resistance cassette (see Dataset EV1). The insertion of the chloramphenicol resistance cassette was verified by PCR.

PilE point mutations

In order to increase transformation efficiency in *N. meningitidis*, we modified the previous vector (TOPO-SB-Kan (Imhaus & Dumenil, 2014)) used for *PilE* mutagenesis as follows: We amplified genomic DNA from the strain transformed with TOPO-SB-Kan by PCR using the primer pair PK-10/21. This fragment was then cloned in TOPO-pCR2.1 (Invitrogen). This plasmid was named TOPO-SB2-Kan and used for *pilE* mutagenesis. To generate point mutations in *pilE*, we used a single-primer one-step mutagenesis process (Huang & Zhang, 2017). Briefly, a mutagenic primer (listed in Dataset EV1) was used to amplify the plasmid TOPO-SB2-Kan by PCR using Phusion polymerase. The PCR product was digested with FastDigest DpnI at 37°C for 8 h and then inactivated at 80°C for 5 min. This product was transformed in XL1 Blue cells, which were then selected on kanamycin-containing LB plates. Plasmids from single colonies were sequenced and transformed in *N. meningitidis* as described above. For primers and strains used in this study see Dataset EV1.

Mutant library generation and analysis

Random mutagenesis was performed using the GeneMorph II Random Mutagenesis Kit. Following manufacturer's instructions, the mutagenic PCR was run with Mutazyme II polymerase using the modified TOPO-SB2-Kan described earlier as a template and primers PK-13 and PK-14. Mutagenic PCR products were purified and used as megaprimers to PCR amplify TOPO-SB-Kan with Phusion polymerase. The PCR product was digested with FastDigest DpnI at 37°C for 8 h and then inactivated at 80°C for 5 min. This product was transformed in XL1 Blue cells and then selected on

Kanamycin-containing LB plates. Mixed plasmids from all the transformants were purified and transformed in *N. meningitidis*. Transformants were selected on plates containing kanamycin, collected the next day, and kept frozen until subjected to selection.

Piliation selection

Bacteria from the library were treated as described in the flow cytometry section. Bacterial suspensions were then sorted with MoFlo® Astrios for 1 h and collected in warm Human Endothelial-SFM + 10% FBS. The sorted population was then plated on kanamycin-containing GCB plates.

Adhesion selection

Bacteria from the library were used to run a 2-h adhesion assay following the protocol described below at the exception that all of the final cell suspension was plated on kanamycin GCB plates.

Aggregation selection

Bacteria from the library were allowed to aggregate at an OD_{600 nm} of 0.6 for 2 h in Millicell Cell Culture Inserts for 24-well plates with a 5 μm pore size. Medium was flown-through several times. The membrane was then vortexed in medium to collect the bacteria, which were then plated. This process was repeated two times to significantly enrich the library in aggregation-positive bacteria. Genomic DNA was then extracted from the different libraries. DNA from each library was amplified by two separate PCR (20 cycles) using two reverse pairs of barcoded primers (primers PK-34 to PK-47) to obtain a more homogeneous coverage upon sequencing. The PCR products were purified, and concentration was normalized using Fragment analyzer (AATI) prior to sequencing. Paired-end sequencing (2 \times 300 bp) was performed using an Illumina Miseq sequencer at the Pasteur genomics platform. Resulting Fastq files were then assembled, filtered, and analyzed for single nucleotide variations using CLC Genomics workbench. Reads are available in BioSample under accession numbers SAMN08971257 to SAMN08971272. The read counts for single amino acid variation were further analyzed using the EdgeR-dedicated script in the SARTools package (Robinson *et al*, 2010; Varet *et al*, 2016). Resulting *P*-values and log values of the ratio were used for downstream analysis.

Each selection was done at least in triplicates on three separate days. The whole selection process was done twice, and the two biological replicates were sequenced twice. This means that we ran a total of 4 sequencing-runs (two biological duplicates and two sequencing duplicates). Exhaustive data (mutation scores and associated *P*-values) are presented in Dataset EV2.

Flow cytometry

Bacteria were resuspended directly from the GCB plates in human endothelial medium + 10% FBS to an OD_{600 nm} of 0.1 and incubated for 30 min at 37°C. Bacterial suspensions were vigorously vortexed, and 1 μl of an antibody mix of 20D9 and anti-mouse IgG (H+L) coupled to Alexa Fluor 488 or 647 each at 100 $\mu\text{g ml}^{-1}$ or 1 μl of an antibody mix of F10-I at 30 $\mu\text{g ml}^{-1}$ and mouse anti-His tag at 100 $\mu\text{g ml}^{-1}$ and anti-mouse IgG (H+L) coupled to Alexa Fluor 488 or 647 at 100 $\mu\text{g ml}^{-1}$ was added to 10 μl of the bacterial suspension and incubated at 37°C for 15 min. 500 μl of warm medium was added to the tubes, samples were briefly vortexed, and samples

were analyzed using a Gallios cytometer (Beckman Coulter). A total of 50,000 events were recorded. Signal was gated in order to exclude cell doublets or bigger aggregates, only removing a small proportion of bacteria.

Aggregation assays

GFP-expressing or Hoechst-labeled bacteria precultured for 2 h up to an $OD_{600\text{ nm}}$ of approximately 0.2 were pelleted (14,200 $\times g$ for 1 min), washed, and concentrated at an $OD_{600\text{ nm}}$ of 0.6 in Human Endothelial-SFM + 10% FBS. 500 μl of this suspension was dispensed in a well of a 96-well μ -plate with square wells (Ibidi). Plates were incubated for 30 min at 37°C in moist atmosphere containing 5% CO_2 , and three fluorescence images per well were captured using a 4 \times objective. The surface covered by bacterial aggregates was quantified in each field of view using a homemade macro in Fiji (Schindelin *et al.*, 2012). Co-aggregation assays were performed similarly to aggregation assays with the exception that bacteria were concentrated to an $OD_{600\text{ nm}}$ of 0.3 and that 250 μl of one bacterial suspension was mixed with 250 μl of another bacterial suspension. Bacterial localization in co-aggregates was determined using the Radial Profile Plot ImageJ plugin on aggregates of similar size.

Adhesion assays

Human umbilical vein endothelial cells (HUVEC, PromoCell) were used between passages 1 and 8 and grown in Human Endothelial-SFM (Gibco) supplemented with 10% heat-inactivated FBS (PAA Laboratories) and 40 $\mu\text{g ml}^{-1}$ of endothelial cell growth supplement (Sigma-Aldrich) and passed every 2–3 days. bEnd.3 cells were grown in DMEM (Gibco) supplemented with 10% heat-inactivated FBS. For 2–4 h adhesion, 10^5 cells were seeded in Costar[®] 24-well TC-Treated plates the day before infection. On the next day, cells were rinsed once and infected with midlog-phase bacteria (multiplicity of infection (MOI) of 100) at 37°C/5% CO_2 . Inoculum was plated and quantified by CFU count. After 30 min of infection, cells were rinsed three times and incubated for 90 min. Again, cells were rinsed three times. Infection was stopped at this stage for 2-h adhesion but pursued for 2 more h for the 4-h adhesion assay. Cells were rinsed three times and incubated in trypsin-EDTA (0.05%) until detached. Trypsin was inactivated by adding culture medium. The infected cells were vortexed and plated at appropriate dilutions on GCB plates. Ratio of CFU after infection over CFU from the inoculum was compared between strains.

For early adhesion assays, 3.5×10^4 cells were seeded in Cellstar[®] 96-well plates (Greiner) the day before infection. On the next day, cells were rinsed once. Hoechst was added to the medium at a final concentration of 1 $\mu\text{g ml}^{-1}$, and cells were infected with midlog-phase GFP-bacteria (MOI 500) for 30 min at 37°C and 5% CO_2 . Wells were rinsed three times and then fixed with 4% formaldehyde for 30 min at room temperature. Wells were rinsed three times with PBS and then imaged with a 40 \times objective. Each infection was run in duplicate, and 16 images were taken per well. A homemade macro in Fiji was used to count the number of bacteria and nuclei per field of view. These values were summed for each well, and a ratio of the total number of bacteria over the total number of nuclei was used to evaluate the number of bacteria per cell.

Scanning electron microscopy of type IV pili

Hydrophilic mixed cellulose esters filters, 13 mm in diameter containing 0.025 μm pores (MF-Millipore, VSWp01300), were placed in 24-well plate, layered with 500 μl of a bacterial suspension at an $OD_{600\text{ nm}}$ of 1 in Human Endothelial-SFM + 10% FBS, and incubated for 30 min at 37°C and 5% CO_2 in a humidified incubator. 500 μl of pre-warmed 8% PFA in 0.1 M HEPES pH 7.4 was then added to the well and incubated at room temperature for 45 min. After three washing steps in HEPES, type IV pili were blocked for 20 min in HEPES-0.2% gelatin (HEPES-G) and incubated with 2 $\mu\text{g ml}^{-1}$ 20D9 antibody followed by 10 $\mu\text{g ml}^{-1}$ goat anti-mouse antibody coupled to Alexa Fluor 568 in HEPES-G, each for 1 h at room temperature. Samples were then post-fixed overnight at 4°C with 2.5% EM-grade glutaraldehyde in HEPES, washed in HEPES, post-fixed in 1% OsO_4 in HEPES for 1 h, washed in distilled water, dehydrated in graded series of ethanol (25, 50, 75, 90, and 100%), critical point dried in liquid CO_2 in a Leica EM CPD300, mounted on aluminum stubs and sputter-coated with 15-nm gold/palladium in a Gatan PEC 682 gun ionic evaporator. Imaging was performed in an Auriga scanning electron microscope (Carl Zeiss) operated at 7 kV with an in-lens secondary electrons detector.

Crude pili preparation

Crude pili preparations were obtained by suspending bacteria to an $OD_{600\text{ nm}}$ of 10 in cold PBS. Bacteria were vortexed for 1 min at maximum speed and then incubated on ice for 2 min. These steps were repeated two more times. To separate pili from debris and bacteria, the suspension was then centrifuged for 5 min at 9,000 $\times g$. This was repeated twice.

Pili under flow

40,000 HUVEC were seeded in Ibidi channels (ibiTreat μ -Slide VI 0.4) 1 day before conducting the experiment. On the next day, crude pili of the reference strain were prepared. Cells were incubated with 5 μl of these preparations for at least 1 h. Channels were washed gently three times with cell culture medium. Pili were then labeled by incubating cells with 20D9 at a final concentration of 2.5 $\mu\text{g ml}^{-1}$ and goat anti-mouse secondary antibody at a final concentration of 5 $\mu\text{g ml}^{-1}$ for at least 15 min at 37°C and 5% CO_2 .

Channels were then perfused using a FlowEz Fluigent pressure-controlled pump. Pressure was computer-controlled using the company-built automation software. Every 30 s, pressure was alternatively turned off or increased by steps of 30 mbar (starting from 55 mbar) for a total duration of 9 min. Flow was then stopped. Cells were imaged every 5 s for a total duration of 10 min using a 40 \times oil immersion objective. Pilus inversion could easily be monitored by visual inspection of the resulting videos, allowing to report threshold pressure values yielding to pilus immobilization.

Flow pressure was converted to shear stress by first estimating the flow using Fluigent's conversion tool. Flow rate was then translated into shear stress using the following equation: $\tau = \eta \cdot 176.1 \cdot \Phi$ based on Ibidi's documentation, where τ is the shear stress (dyn cm^{-2}), η is the dynamical viscosity of the medium (dyns cm^{-2}), and Φ is the flow rate (ml min^{-1}).

Pili purification

Pili used for Western blots and mass spectrometry were prepared as described previously (Gault *et al*, 2015). Briefly, bacteria from 10 to 12 petri dishes were harvested in 5 mL of 150 mM ethanolamine at pH 10.5. Pili were sheared by vortexing for 1 min. Bacteria were centrifuged at 4,000 $\times g$ for 30 min at 4°C, and the resulting supernatant further centrifuged at 15,000 $\times g$ for 30 min at room temperature. The supernatant was removed, pili precipitated from the suspension by the addition of 10% (vol/vol) ammonium sulfate saturated in 150 mM ethanolamine pH 10.5 and allowed to stand for 1 h. The precipitate was pelleted by centrifugation at 4,000 $\times g$ for 1 h at 20°C. Pellets were washed twice with PBS and suspended in 100 μ l distilled water.

Mass spectrometry analysis

Samples were analyzed in LC-MS using a Dionex UltiMate 3000 RSLC Nano System coupled to an Orbitrap Fusion Lumos mass spectrometer fitted with a nano-electrospray ionization source (Thermo Scientific). 5 μ l of protein sample was loaded at a flow rate of 5 μ l min⁻¹ onto an in-house packed C4 (5 μ m, Reprosil) trap column (0.150 mm i.d. \times 35 mm) and separated at a flow rate of 0.5 μ l min⁻¹ using a C4 (5 μ m, Reprosil) column (0.075 mm i.d. \times 340 mm). The following gradient was used: 2.0% B from 0 to 7 min; 35% B at 8 min.; 60% B at 20 min.; 99% B from 30 to 34 min.; and 2.0% B from 34.1 to 50 min. Solvent A consisted of 98% H₂O, 2% ACN, and 0.1% FA, and solvent B consisted of 20% H₂O, 80% ACN, and 0.1% FA.

MS scans were acquired at 120,000 resolving power (at m/z 400) with a scan range set to 550–1,750 m/z , five microscans (μ scans) per MS scan, an automatic gain control (AGC) target value of 5×10^5 , and maximum injection time of 50 ms. All MS scans were charge-state deconvoluted and deisotoped with XTRACT in Proteome Deconvolution 3.0 (Thermo Scientific) (70% fit factor, minimum S/N = 2, remainder threshold = 10%, minimum of three detected charge states, and a charge range of + 5 to + 30). Relative abundance was calculated using an extracted ion chromatogram (XIC) for each protein.

Immunofluorescence

For immunofluorescence, samples were fixed with PBS containing 4% formaldehyde for 30 min at room temperature. After rinsing, samples were blocked in PBS containing 0.2% skin fish gelatin (PBSG) for 30 min. Samples were then incubated with appropriate combinations of the following: 20D9 diluted in PBSG at 2.5 μ g ml⁻¹ and/or SM1 diluted at 2 μ g ml⁻¹ or F10-I diluted at 4 μ g ml⁻¹ for 1 h and subsequently incubated with the secondary antibody anti-mouse-Alexa Fluor 491 or 568 diluted in PBSG at 10 μ g ml⁻¹ and/or DyLight 650 (Invitrogen) conjugated mouse anti-His tag for 1 h at room temperature or overnight at 4°C.

Quantification of piliation by microscopy

Bacteria were precultured for 2 h in endothelial cell culture medium. Bacterial suspensions were normalized to an OD_{600 nm} of 0.2 and dispensed in Ibidi channels (Ibidi Treat μ -Slide VI 0.4) and incubated for 30 min at 37°C and 5% CO₂. Bacteria were then rinsed

four times with PBS to recover adherent bacteria only. Samples were then stained with 20D9 and DAPI as described in the immunofluorescence section. Over 100 images were captured for each sample using a 100 \times oil immersion objective. Quantification of piliation on individual bacteria was performed automatically using a custom-built Fiji macro (available upon request) taking advantage of the Ridge Detection plugin. Downstream data analysis was only performed on piliated bacteria.

SDS-PAGE and Western blot

Protein samples preparation, SDS-PAGE separation, transfer, and immunoblotting were performed using standard biochemistry techniques (Harlow & Lane, 1976 a Laboratory Manual). Proteins were separated by SDS-PAGE in Tris-glycine gels containing 12–15% polyacrylamide and transferred onto PVDF membranes (Thermo Scientific) using semi-dry electrotransfer (Bio-Rad). Membranes were blocked with PBS + 0.1% Tween-20 + 5% milk for 30 min and incubated for 1 h with polyclonal antibodies (anti-PilE at 1/5,000; anti-PilV at 1/1,500) diluted in blocking solution. Membranes were then incubated with horseradish peroxidase (HRP)-coupled anti-rabbit antibody (1/10,000) in blocking solution. Peroxidase activity was detected by enhanced chemiluminescence (ECL-plus, Pierce) and recorded with a G:BOX Chemi multi-purpose imaging system from Syngene. Protein quantities were analyzed using the Fiji software.

Statistical analysis

GraphPad was used to plot graphs and run appropriate statistical tests. Paired *t*-test was used in Figs EV1G and I, and EV2C and EV3C–F, and EV4B and C, and one-way ANOVA was used in Figs 2E and 3E, and 4D and E, and 5G, and EV2D and F. Statistical significance was defined by $P < 0.05$ (*), $P < 0.01$ (**), and $P < 0.001$ (***)

Expanded View for this article is available online.

Acknowledgements

This work was supported by the Integrative Biology of Emerging Infectious Diseases (IBEID) laboratory of excellence; the VIP European Research Council starting grant (GD); Paris Descartes University PhD fellowship, the FRM PhD fellowship (FDT20170437205), and Programme Bettencourt (Ecole Doctorale Frontières du Vivant, FdV) funding. NGS was performed at the Genomics Platform, member of "France Génomique" consortium (ANR10-INBS-09-08). We acknowledge the Ultrapole platform and cytometry platform of the Center for Innovation and Technological Research (CRT) at Institut Pasteur for support in conducting this study. We would like to thank Mumtaz Virji and Darryl J Hill for providing the SM1 antibody. We are also extremely grateful to Daria Bonazzi, Dorian Obino, and Olivera Francetic for critical reading of the manuscript and to all members of the Dumenil laboratory for helpful discussions.

Author contributions

PK and GD designed research. PK, AC-O SG, and A-FI performed experiments. MD and JC-R provided the mass spectrometry analysis. DN provided the physical model of pilus adhesion under flow. PK and GD wrote the manuscript with help for the figures from AC-O.

Conflict of interest

The authors declare that they have no conflict of interest.

References

- Beaussart A, Baker AE, Kuchma SL, El-Kirat-Chatel S, O'Toole GA, Dufrene YF (2014) Nanoscale adhesion forces of *Pseudomonas aeruginosa* type IV Pili. *ACS Nano* 8: 10723–10733
- Berry JL, Pelicic V (2015) Exceptionally widespread nanomachines composed of type IV pilins: the prokaryotic Swiss Army knives. *FEMS Microbiol Rev* 39: 134–154
- Biais N, Higashi DL, Brujic J, So M, Sheetz MP (2010) Force-dependent polymorphism in type IV pili reveals hidden epitopes. *Proc Natl Acad Sci USA* 107: 11358–11363
- Blake MS, MacDonald CM, Klugman KP (1989) Colony morphology of pilated *Neisseria meningitidis*. *J Exp Med* 170: 1727–1736
- Bonazzi D, Lo Schiavo V, Machata S, Djafer-Cherif I, Nivoit P, Manriquez V, Tanimoto H, Husson J, Henry N, Chate H et al (2018) Intermittent pili-mediated forces fluidize *Neisseria meningitidis* aggregates promoting vascular colonization. *Cell* 174: 143–155 e16
- Brissac T, Mikaty G, Dumenil G, Coureuil M, Nassif X (2012) The meningococcal minor pilin PilX is responsible for type IV pilus conformational changes associated with signaling to endothelial cells. *Infect Immun* 80: 3297–3306
- Chamot-Rooke J, Rousseau B, Lanterrier F, Mikaty G, Mairey E, Malosse C, Bouchoux G, Pelicic V, Camoin L, Nassif X et al (2007) Alternative *Neisseria* spp. type IV pilin glycosylation with a glyceramido acetamido trideoxyhexose residue. *Proc Natl Acad Sci USA* 104: 14783–14788
- Chamot-Rooke J, Mikaty G, Malosse C, Soyer M, Dumont A, Gault J, Imhaus AF, Martin P, Trellet M, Clary G et al (2011) Posttranslational modification of pili upon cell contact triggers *N. meningitidis* dissemination. *Science* 331: 778–782
- Charles-Orszag A, Tsai FC, Bonazzi D, Manriquez V, Sachse M, Mallet A, Salles A, Melican K, Staneva R, Bertin A et al (2018) Adhesion to nanofibers drives cell membrane remodeling through one-dimensional wetting. *Nat Commun* 9: 4450
- Chen A, Seifert HS (2014) Saturating mutagenesis of an essential gene: a majority of the *Neisseria gonorrhoeae* major outer membrane porin (PorB) is mutable. *J Bacteriol* 196: 540–547
- Chiang SL, Taylor RK, Koomey M, Mekalanos JJ (1995) Single amino acid substitutions in the N-terminus of *Vibrio cholerae* TcpA affect colonization, autoagglutination, and serum resistance. *Mol Microbiol* 17: 1133–1142
- Coureuil M, Lecuyer H, Scott MG, Boularan C, Enslin H, Soyer M, Mikaty G, Bourdoulous S, Nassif X, Marullo S (2010) Meningococcus Hijacks a beta2-adrenoceptor/beta-Arrestin pathway to cross brain microvasculature endothelium. *Cell* 143: 1149–1160
- De Baets G, Schymkowitz J, Rousseau F (2014) Predicting aggregation-prone sequences in proteins. *Essays Biochem* 56: 41–52
- van Deuren M, Brandtzaeg P, van der Meer JW (2000) Update on meningococcal disease with emphasis on pathogenesis and clinical management. *Clin Microbiol Rev* 13: 144–166
- Fowler DM, Fields S (2014) Deep mutational scanning: a new style of protein science. *Nat Methods* 00: 801–807
- Gault J, Ferber M, Machata S, Imhaus AF, Malosse C, Charles-Orszag A, Millien C, Bouvier G, Bardiaux B, Pehau-Arnaudet G et al (2015) *Neisseria meningitidis* type IV pili composed of sequence invariable pilins are masked by multisite glycosylation. *PLoS Pathog* 11: e1005162
- Georgiadou M, Castagnini M, Karimova G, Ladant D, Pelicic V (2012) Large-scale study of the interactions between proteins involved in type IV pilus biology in *Neisseria meningitidis*: characterization of a subcomplex involved in pilus assembly. *Mol Microbiol* 84: 857–873
- Giltner CL, Habash M, Burrows LL (2010) *Pseudomonas aeruginosa* minor pilins are incorporated into type IV pili. *J Mol Biol* 398: 444–461
- Harlow E, Lane D (1976) Adrenergic stimulants (or sympathomimetic medicines). *Rev Infirm* 26: 75–78
- Helaine S, Carbonnelle E, Prouvensier L, Beretti JL, Nassif X, Pelicic V (2005) PilX, a pilus-associated protein essential for bacterial aggregation, is a key to pilus-facilitated attachment of *Neisseria meningitidis* to human cells. *Mol Microbiol* 55: 65–77
- Helaine S, Dyer DH, Nassif X, Pelicic V, Forest KT (2007) 3D structure/function analysis of PilX reveals how minor pilins can modulate the virulence properties of type IV pili. *Proc Natl Acad Sci USA* 104: 15888–15893
- Hospenthal MK, Waksman G (2019) The remarkable biomechanical properties of the type 1 chaperone-usher pilus: a structural and molecular perspective. *Microbiol Spectr* 7: 1–10
- Huang Y, Zhang L (2017) *An in vitro* single-primer site-directed mutagenesis method for use in biotechnology. New York, NY: Humana Press, 375–383
- Imhaus AF, Dumenil G (2014) The number of *Neisseria meningitidis* type IV pili determines host cell interaction. *EMBO J* 33: 1767–1783
- Jolley KA, Maiden MC (2010) BIGSdb: scalable analysis of bacterial genome variation at the population level. *BMC Bioinformatics* 11: 595
- Kellogg DS Jr, Cohen IR, Norins LC, Schroeter AL, Reising G (1968) *Neisseria gonorrhoeae*. II. Colonial variation and pathogenicity during 35 months *in vitro*. *J Bacteriol* 96: 596–605
- Kilmury SL, Burrows LL (2016) Type IV pilins regulate their own expression via direct intramembrane interactions with the sensor kinase PilS. *Proc Natl Acad Sci USA* 113: 6017–6022
- Kolappan S, Coureuil M, Yu X, Nassif X, Egelman EH, Craig L (2016) Structure of the *Neisseria meningitidis* type IV pilus. *Nat Commun* 7: 13015
- Korotkov KV, Hol WG (2008) Structure of the GspK-GspI-GspJ complex from the enterotoxigenic *Escherichia coli* type 2 secretion system. *Nat Struct Mol Biol* 15: 462–468
- Lu S, Giuliani M, Harvey H, Burrows LL, Wickham RA, Dutcher JR (2015) Nanoscale pulling of type IV pili reveals their flexibility and adhesion to surfaces over extended lengths of the pili. *Biophys J* 108: 2865–2875
- Marceau M, Beretti JL, Nassif X (1995) High adhesiveness of encapsulated *Neisseria meningitidis* to epithelial cells is associated with the formation of bundles of pili. *Mol Microbiol* 17: 855–863
- Melican K, Michea Veloso P, Martin T, Bruneval P, Dumenil G (2013) Adhesion of *Neisseria meningitidis* to dermal vessels leads to local vascular damage and purpura in a humanized mouse model. *PLoS Pathog* 9: e1003139
- Merz AJ, So M, Sheetz MP (2000) Pilus retraction powers bacterial twitching motility. *Nature* 407: 98–102
- Mikaty G, Soyer M, Mairey E, Henry N, Dyer D, Forest KT, Morand P, Guadagnini S, Prevost MC, Nassif X et al (2009) Extracellular bacterial pathogen induces host cell surface reorganization to resist shear stress. *PLoS Pathog* 5: e1000314
- Morand PC, Tattevin P, Eugene E, Beretti JL, Nassif X (2001) The adhesive property of the type IV pilus-associated component PilC1 of pathogenic *Neisseria* is supported by the conformational structure of the N-terminal part of the molecule. *Mol Microbiol* 40: 846–856
- Morand PC, Bille E, Morelle S, Eugene E, Beretti JL, Wolfgang M, Meyer TF, Koomey M, Nassif X (2004) Type IV pilus retraction in pathogenic *Neisseria* is regulated by the PilC proteins. *EMBO J* 23: 2009–2017

- Nassif X, Lowy J, Stenberg P, O'Gaora P, Ganji A, So M (1993) Antigenic variation of pilin regulates adhesion of *Neisseria meningitidis* to human epithelial cells. *Mol Microbiol* 8: 719–725
- Nassif X, Beretti JL, Lowy J, Stenberg P, O'Gaora P, Pfeifer J, Normark S, So M (1994) Roles of pilin and PilC in adhesion of *Neisseria meningitidis* to human epithelial and endothelial cells. *Proc Natl Acad Sci USA* 91: 3769–3773
- Nguyen Y, Harvey H, Sugiman-Marangos S, Bell SD, Buensuceso RN, Junop MS, Burrows LL (2015) Structural and functional studies of the *Pseudomonas aeruginosa* minor pilin, PilE. *J Biol Chem* 290: 26856–26865
- Novotny LA, Jurcisek JA, Ward MO Jr, Jordan ZB, Goodman SD, Bakaletz LO (2015) Antibodies against the majority subunit of type IV Pili disperse nontypeable *Haemophilus influenzae* biofilms in a LuxS-dependent manner and confer therapeutic resolution of experimental otitis media. *Mol Microbiol* 96: 276–292
- Obergfell KP, Seifert HS (2016) The pilin N-terminal domain maintains *neisseria gonorrhoeae* transformation competence during pilus phase variation. *PLoS Genet* 12: e1006069
- Park HS, Wolfgang M, van Putten JP, Dorward D, Hayes SF, Koomey M (2001) Structural alterations in a type IV pilus subunit protein result in concurrent defects in multicellular behaviour and adherence to host tissue. *Mol Microbiol* 42: 293–307
- Pujol C, Eugene E, Marceau M, Nassif X (1999) The meningococcal PilT protein is required for induction of intimate attachment to epithelial cells following pilus-mediated adhesion. *Proc Natl Acad Sci USA* 96: 4017–4022
- Robinson MD, McCarthy DJ, Smyth GK (2010) edgeR: a bioconductor package for differential expression analysis of digital gene expression data. *Bioinformatics* 26: 139–140
- Rudel T, Scheurerpflug I, Meyer TF (1995) *Neisseria* PilC protein identified as type-4 pilus tip-located adhesin. *Nature* 373: 357–359
- Schindelin J, Arganda-Carreras I, Frise E, Kaynig V, Longair M, Pietzsch T, Preibisch S, Rueden C, Saalfeld S, Schmid B et al (2012) Fiji: an open-source platform for biological-image analysis. *Nat Methods* 9: 676–682
- Seifert HS, Ajioka RS, Paruchuri D, Heffron F, So M (1990) Shuttle mutagenesis of *Neisseria gonorrhoeae*: pilin null mutations lower DNA transformation competence. *J Bacteriol* 172: 40–46
- Skerker JM, Berg HC (2001) Direct observation of extension and retraction of type IV pili. *Proc Natl Acad Sci USA* 98: 6901–6904
- Tala L, Fineberg A, Kukura P, Persat A (2019) *Pseudomonas aeruginosa* orchestrates twitching motility by sequential control of type IV pili movements. *Nat Microbiol* 4: 774–780
- Tan FY, Wormann ME, Loh E, Tang CM, Exley RM (2015) Characterization of a novel antisense RNA in the major pilin locus of *Neisseria meningitidis* influencing antigenic variation. *J Bacteriol* 197: 1757–1768
- Varet H, Brillet-Gueguen L, Coppee JY, Dillies MA (2016) SARTools: a DESeq2- and EdgeR-Based R pipeline for comprehensive differential analysis of RNA-Seq data. *PLoS ONE* 11: e0157022
- Virji M, Heckels JE, Watt PJ (1983) Monoclonal antibodies to gonococcal pili: studies on antigenic determinants on pili from variants of strain P9. *J Gen Microbiol* 129: 1965–1973
- Winther-Larsen HC, Hegge FT, Wolfgang M, Hayes SF, van Putten JP, Koomey M (2001) *Neisseria gonorrhoeae* PilV, a type IV pilus-associated protein essential to human epithelial cell adherence. *Proc Natl Acad Sci USA* 98: 15276–15281
- Wolfgang M, van Putten JP, Hayes SF, Koomey M (1999) The comp locus of *Neisseria gonorrhoeae* encodes a type IV prepilin that is dispensable for pilus biogenesis but essential for natural transformation. *Mol Microbiol* 31: 1345–1357
- Woods DE, Straus DC, Johanson WG Jr, Berry VK, Bass JA (1980) Role of pili in adherence of *Pseudomonas aeruginosa* to mammalian buccal epithelial cells. *Infect Immun* 29: 1146–1151